

Development of a Scalable Fabrication Concept for Sustainable, Programmable Shape-Morphing Metamaterials

Angela Schwarz,* Tobias Lichti, Franziska Wenz, Benedikt M. Scheuring, Christof Hübner, Christoph Eberl, and Peter Elsner

Programmable materials are a novel development, in which specialized production processes are used to introduce a framework of information capabilities into the inner structure of materials. Since the design and fabrication of programmable materials are still challenging, this aims to introduce a design and fabrication concept to pave the way toward industrial application. Herein, complex shape morphing has been implemented in the sense that the shape changes in response to external conditions, following a predefined program. First, the feasibility of a fabrication concept for uniform metamaterials with auxetic behavior is presented. A material with a predetermined nonuniform inner structure that deforms to a symmetrical shape has been developed and fabricated according to this concept. More complex behavior can be implemented by facilitating optimization methods to find inner structures according to a target shape. Lastly, an optimized and producible design for asymmetrical shape morphing is described to demonstrate the applicability of the approach.

introduced on the molecular and mesoscopic levels.^[2] The algorithms can be used to implement shape morphing, adaptive stiffness or even self-repair.^[3] Here, for example, changes in the local state are used as if-then-else conditions (or other equivalents of logical gates). *Meta-* or bistable states for material memory and the designability of local functional dependencies between a global input and a local output (in this article: longitudinal vs transversal strain) complete the basic elements to implement simple information processing.^[2,4,5] For example, in the field of advanced robotics, the need for distributed information processing and actuation has been identified as the main challenge in materials robotics.^[6]

While the challenges associated with designing materials behavior at the molecular and atomistic levels are the long story of materials science, the design space on the mesoscopic level has been significantly enhanced by the introduction of metamaterials. To narrow down the scope of this article, the focus will be on the material's behavior of structural materials and specifically manufacturable programmable mechanical metamaterials.


Mechanical metamaterials still pose challenges regarding their conceptual design, the definition of the required properties,

1. Introduction

Resource scarcity, challenges in up- or recycling of materials as well as function integration in industrial applications require novel materials concepts.^[1] One framework capable of introducing information processing and an adjustable reaction to external forces or fields is programmable materials. Such materials allow algorithms to be instantiated by the use of mechanisms

A. Schwarz, C. Hübner
Polymer Engineering
Fraunhofer Institute for Chemical Technology (ICT)
Joseph-von-Fraunhofer-Str. 7, 76327 Pfinztal, Germany
E-mail: angela.schwarz@ict.fraunhofer.de

T. Lichti
Flow and Material Simulation
Fraunhofer Institute for Industrial Mathematics (ITWM)
Fraunhofer-Platz 1, 67663 Kaiserslautern, Germany

 The ORCID identification number(s) for the author(s) of this article can be found under <https://doi.org/10.1002/adem.202200386>.

© 2022 The Authors. Advanced Engineering Materials published by Wiley-VCH GmbH. This is an open access article under the terms of the Creative Commons Attribution-NonCommercial-NoDerivs License, which permits use and distribution in any medium, provided the original work is properly cited, the use is non-commercial and no modifications or adaptations are made.

†Deceased May 2022

DOI: 10.1002/adem.202200386

F. Wenz, C. Eberl
Component Safety and Lightweight Construction
Fraunhofer Institute for Mechanics of Materials (IWM)
Wöhlerstraße 11, 79108 Freiburg, Germany

F. Wenz, C. Eberl
IMTEK
Uni-Freiburg
Georges-Köhler-Allee 078, 79110 Freiburg, Germany

B. M. Scheuring
Hybrid and Lightweight Materials
Karlsruhe Institute of Technology - Institute for Applied Materials (IAM)
Engelbert-Arnold-Straße 4, 76131 Karlsruhe, Germany

P. Elsner†
Institute Director
Fraunhofer Institute for Chemical Technology (ICT)
Joseph-von-Fraunhofer-Str. 7, 76327 Pfinztal, Germany

P. Elsner†
Member of Directorate Board
Karlsruhe Institute of Technology - Institute for Applied Materials (IAM)
Engelbert-Arnold-Straße 4, 76131 Karlsruhe, Germany

their fabrication, and therefore their applicability in the industry.^[7,8]

Built on conventional unit cell-based mechanical metamaterials, Programmable materials express a designed behavior that can be adapted by a local change of the material's inner structure according to an a priori-defined requirement. Due to their geometry, the underlying unit cells have adjustable features, which are used to control the local properties of the material. A reversible and local material behavior like shape morphing can be implemented using cell geometries with different Poisson ratios that are locally adjustable.^[9,10]

With these features, programmable materials have the potential to transfer system functionalities like load-dependent if–then–else deformations to the material level, because the properties of a component are not limited by the properties of the base material.^[2,4,11]

One of the best-known metamaterials is the Miura-ori folding which is origami based. Its macroscopic properties are scale independent^[12–14] and widely determined by its inner structure, e.g., the position of folding edges or wall thickness, instead of the properties of the base material alone.^[15] The structure can be divided into so-called unit cells that are a repeating element in the building of a metamaterial. It is therefore possible to carry out a targeted variation of the design parameters of the unit cells and to program them in a material. Nevertheless, when three-dimensional metamaterial structures^[16] are designed with variations in their inner structure, a numerical analysis with a fully resolved model is very time-consuming. For that reason, several numerical homogenization methods^[17–19] have been developed to study heterogeneous materials. One approach is to establish a surrogate model for finite deformations by precomputing the homogenized properties of a representative volume element (RVE), in our case corresponding to a unit cell, for several load cases.^[19] To find an optimal and application-oriented structure design according to individual requirements for shape morphing and production restrictions, homogenization and optimization techniques can be combined.^[20] Numerical analysis and design development are closely related to the fabrication of complex inner structures, since the conditions of manufacturability represent the limit in the development. Until now, single layers of Miura-ori foldings are often fabricated with processes like additive manufacturing,^[21] casting processes,^[22] or pressing methods.^[23] The disadvantages of these processes are that additive methods are time-consuming and often only suitable for the research sector, and the other two processes use complex molds.^[22,23] However, an optimization of the structure regarding functionalization increases the structural complexity and thus reduces their manufacturability for industrial applications.^[7]

This article shows a fabrication concept of a programmable material with an optimized shape morphing based on a large 3D array of Miura-ori unit cells. First, a fabrication concept suitable for a possible mass production of such a material is developed. Second, the cell geometries needed to be designed for this fabrication methodology, and the material's structural logic instantiated across the material's volume. Third, surrogate-based optimization is used to find the desired geometry for each cell within the material's volume to account for boundary conditions and more complex shape morphing. The model is validated against classical finite element methods (FEM) and experimental results. We show that the chosen fabrication

concept allows the production of large 3D mono-material volumes, which can express complex shape morphing behavior based on the instantiated logic and functional dependencies.

2. Definition of the Unit Cell Geometry

All metamaterial volumes manufactured for this article were developed based on a unit cell, which can be manufactured from foil structuring and stacking. The chosen unit cell structure is derived from Miura-ori folding^[16] and consists of four connected parallelograms, where the connected edges act as long joints, resulting in a foldable structure, **Figure 1a**. The deformation behavior of the material's volume is determined by the unit cells and thus by the shape of these parallelograms and since the material is in reality not infinitely compliant, the “starting” angle of the joints.

The unit cell geometry consists of two layers and is shown in **Figure 1**. h is the total unit cell height, $2S$ the width, and $2L$ the length. The stacked layers are described by the geometry of the unit cell which built them up, where h_1 is the height of the part-unit cell in the upper layer and h_2 the height of the part-unit cell in the lower layer, shown in **Figure 1b**. The parameter V is the offset between the end point of the diagonal and the tip of the part-unit cell. For a complete description of the unit cell geometry, we refer to Schenk et al.^[24] The in-plane auxetic folding behavior is described by a negative Poisson's ratio

$$\nu_{SL} = -\frac{S dL}{L dS} \quad (1)$$

which depends on the width and length of the part-unit cell.^[16] In the x/z -plane, multiple Miura-ori-based part-unit cells can be connected to a uniform unit cell array with an in-plane auxetic behavior, as shown in **Figure 1c** (top). Further, uniform unit cell arrays can be stacked at different heights in the y -direction resulting in a 3D metamaterial structure^[16,24–26] see **Figure 1c** (bottom). To obtain a connected array of cells on a cartesian grid, it must be ensured, that the outer dimensions of each unit cell are the same. For this reason, the following conditions must apply

$$\begin{aligned} \Delta h &= h_1 - h_2 > 0 = \text{const} \\ S &= \text{const} \\ L &= \text{const} \end{aligned} \quad (2)$$

Under consideration of Equation (2) and **Figure 1a,b**, the parameters V and h_2 (or h_1) remain variable and can be used as design variables for the unit cell. In **Figure 1d** the offset parameter V is continuously changing along the array and forms a nonuniform part-unit cell array. The geometry parameters of each cell and the different values of V for the nonuniform part-unit cell array shown in **Figure 1d** can be found in the Supporting Information.

The influence of both design parameters, V and h_2 , on the unit cell's effective behavior, is shown in **Figure 2**. Increasing the offset parameter V leads to a larger auxetic deformation in the z -direction under strain in the x -direction shown in **Figure 2a** and can be used to program a specific shape under a load in the x -direction. As soon as this layer is completely stretched, the Poisson's ratio changes from negative to positive (see

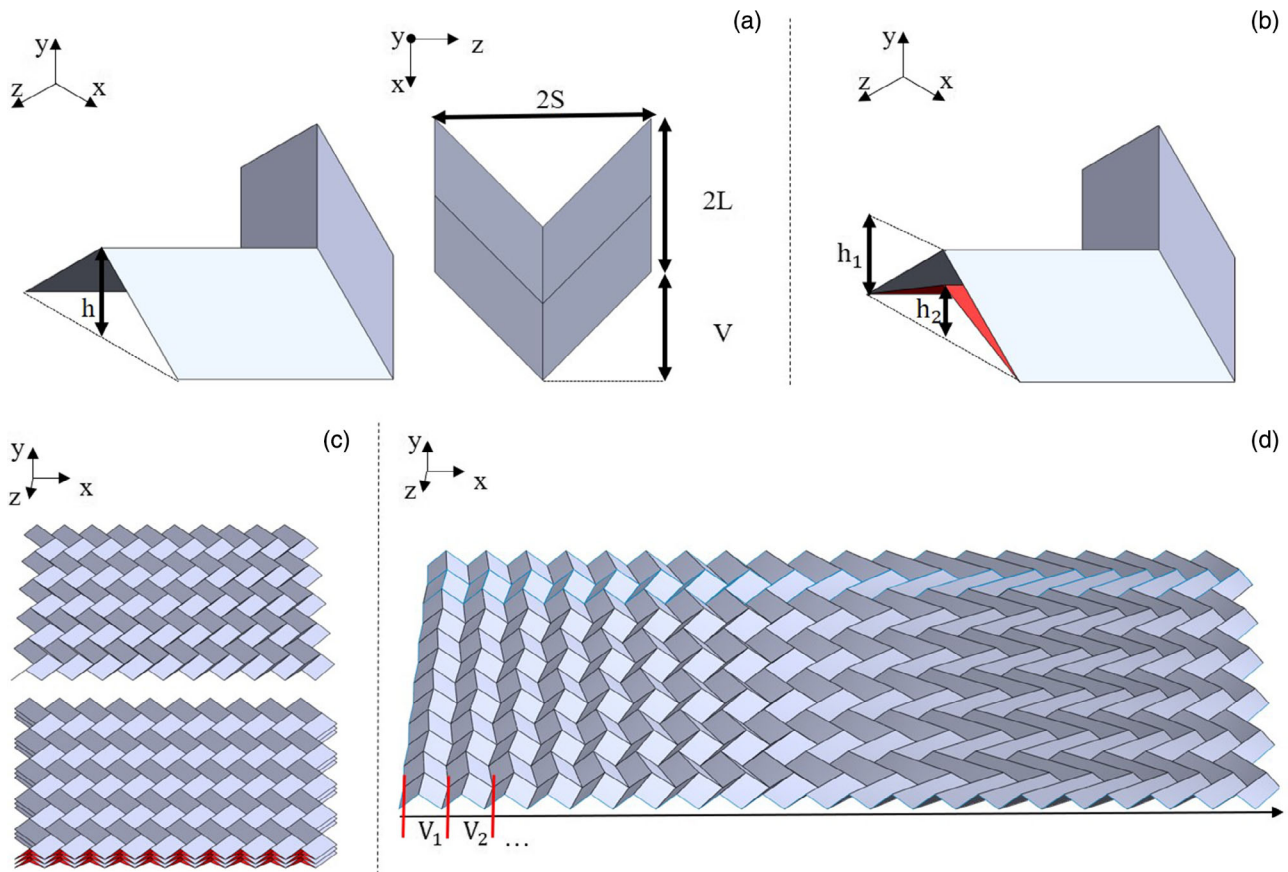


Figure 1. a) Part-unit cell, b) unit cell, c) uniform part-unit cell array (top) and uniform unit cell array (bottom), d) nonuniform part-unit cell array.

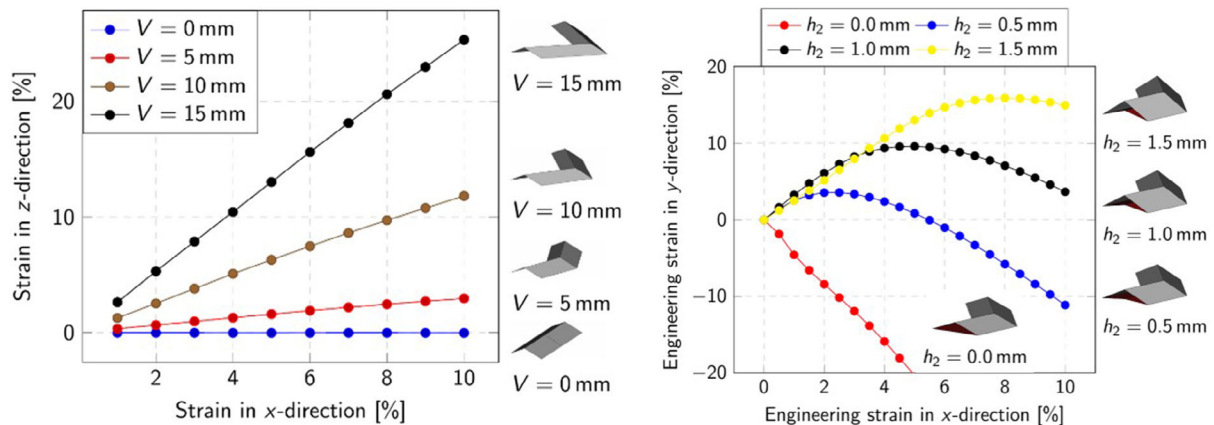


Figure 2. Influence of the design parameters on the macroscopic mechanical behavior of the unit cell under strain in the x-direction. Influence of V on the transversal strain in the z-direction (left). Influence of h_2 on the transversal strain in the y-direction (right).

Figure 2b). Due to the variance of the offsets V , neighboring cells are slightly different in length. For this reason, the vertices and edges that are shared by neighboring cells must be adjusted by averaging the different V of the neighboring cells. Consequently, a part-unit cell may have another V on its left and right side and is slightly distorted. The difference in V of neighboring part-unit cells should be sufficiently low such that the structure can be assumed to be periodic in a near neighborhood.

3. Results and Discussions

3.1. Fabrication Concept for Structures with Variable Design Parameters

To be able to manufacture complex parameterized 3D structures from optimization as described in Section 5.2, a manufacturing concept suitable for mass production was developed. Classical

production methods for metamaterials are additive manufacturing methods like 3D printing. Such technologies are rather suitable for new product development with low production volumes and high complexity due to cost reduction than for mass production.^[7,27–29]

Hence, in this work, the inner structure of the programmable materials is separated into different structured layers which are easy to assemble by layer stacking which enables a fast, adaptable, and cost-efficient production. **Figure 3** shows schematically the way from the vision to industrial application with the interaction between optimization and fabrication and the detailed fabrication steps for mass production.

In the first step, the design parameters for shape morphing are specified according to the requirement (Figure 3a). After that thermoforming molds are produced by 3D printing from ABS material (Figure 3b). A re-use of the molds is repeated up to 20 times, before the wear of the molding material is too high. The production of the individual layers is carried out in the thermoforming process (Figure 3c). Solvent welding is used for joining the structured layers (Figure 3d) by applying the solution punctually to the “hills” and “valleys” of the higher and the lower structured layers using a syringe with a 0.1 mm cannula. For the solvent welding, 15% of the TPU is solved in dimethylformamide and results in an average viscosity of 611 mPa·s in the shear rate range of $1\text{--}10^3\text{ s}^{-1}$ and a temperature of 20 °C. This connection technique offers a very good adhesion quality and a high potential for automation. Additionally, this method leads to a mono-material structure, which ensures recyclability. In the Supporting Information, the detailed preparation process for connecting the stacked individual layer is described.

To stabilize the structured layers mechanically during stacking, a support is used for guiding them on top of each other in a stabilized manner and subsequently joined under 50 N joining pressure. To check the joint quality, tensile peel tests were carried out on joined films according to DIN 1465 and on structured double layers, which can be found in the Supporting Information. In both cases, failure occurred in the material before the joints failed, due to the physically entangled polymer chains caused by the solvent welding. To produce higher stackings, the double layers created in this way are joined in subsequent processes (Figure 3e).

With this manufacturing concept, it is possible to produce programmable materials on a large scale from only a single based material. This opens the way to industrial applicability in the various fields of application.

3.2. Simulation and Experimental Validation of a Uniform and Nonuniform Structure

Section 5.2 elaborates on the possibility to arrange the Miura-Ori-based cells in an array, leading to complex geometries with a hierarchical architecture. However, due to the parametrization of each cell in the array, there are numerous design possibilities. First, the cell geometry and the requirements for aligning parametrized cells in an array are described. Next, the simulation and optimization techniques, used to exploit the whole design space under consideration of the complex structure are briefly described.

To validate the programmable materials behavior, different examples of stacked uniform unit cell arrays and non-uniform unit cell arrays have been characterized. In all cases, tension

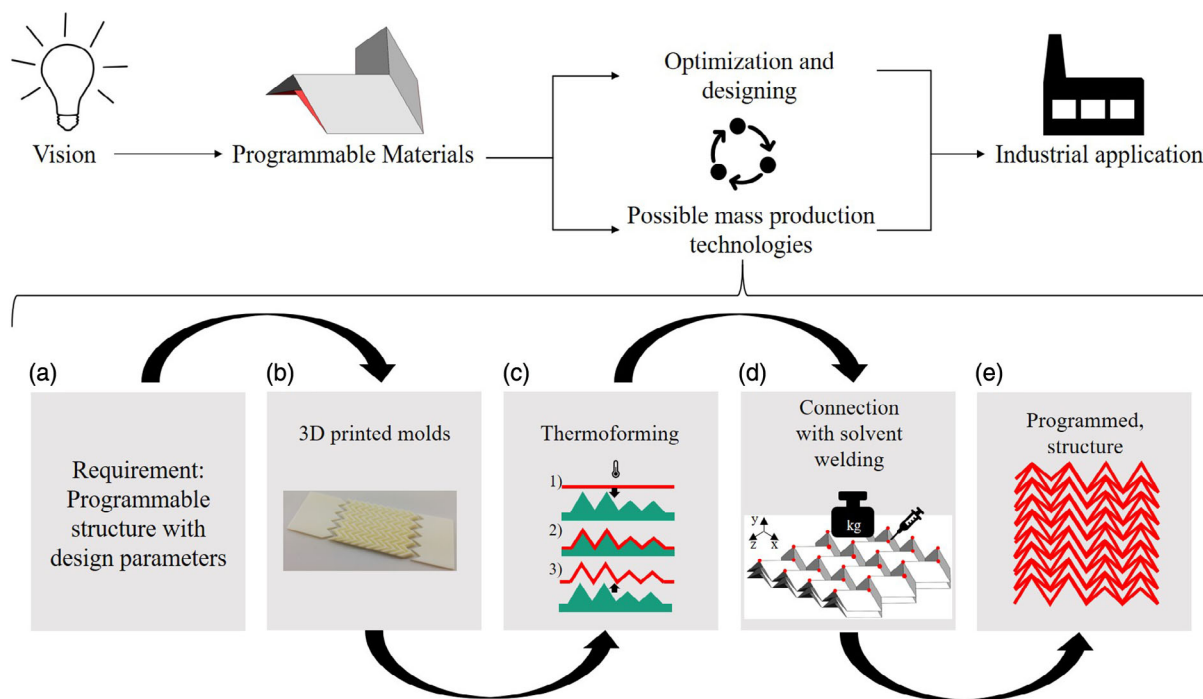


Figure 3. Fabrication concept: a) identifying requirements and mold design, b) 3D-printed molds with adapter plates, c) thermoforming process, d) joining of layers with positive and negative shapes, e.g., different wall thicknesses, e) stacking of the layers via solvent welding.

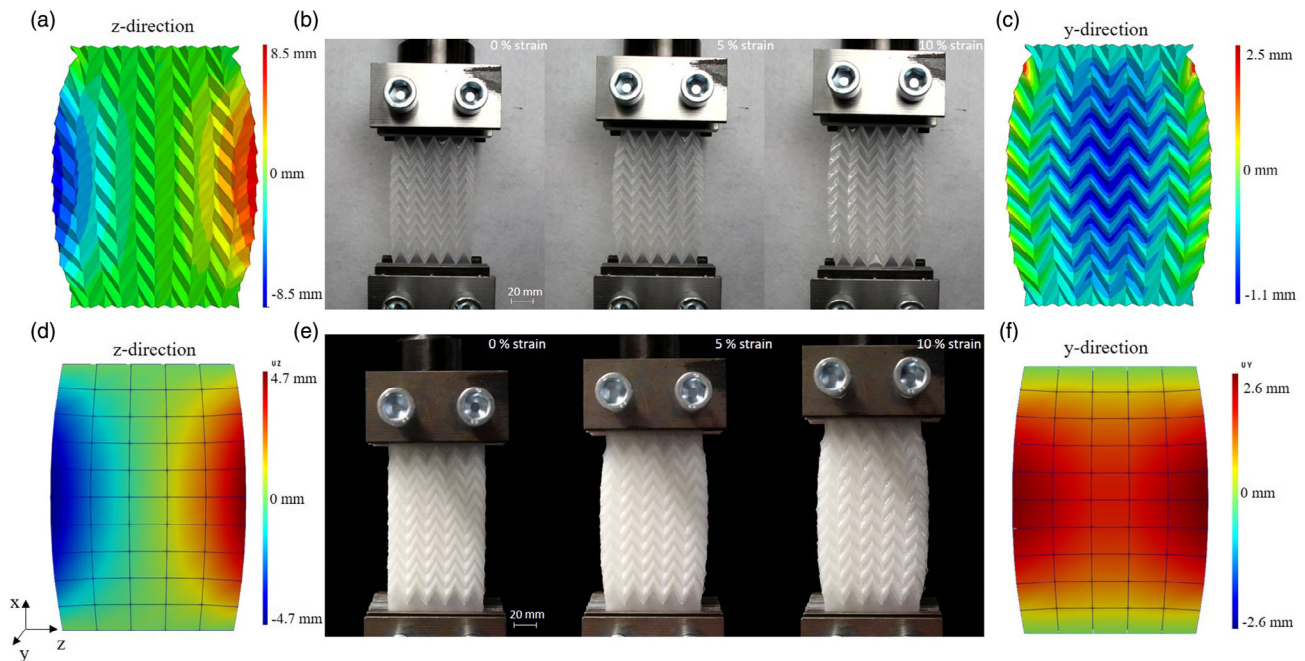


Figure 4. Uniform part-unit cell array at a strain of 10% in the x -direction: a) simulation of the displacement in the z -direction (fully resolved simulation), b) tensile test with increasing out-of-plane and in-plane movement (occurring reflections in the two rightmost pictures), c) simulation of the displacement in the y -direction with curving out-of-plane (fully resolved simulation); 40-layered uniform unit cell array at a strain of 10% in the x -direction: d) displacement in the z -direction (surrogate simulation), e) tensile test without increasing out-of-plane and in-plane movement, f) displacements in the y -direction (surrogate simulation).

in the x -direction is applied and the in-plane displacements in the z -direction are compared to simulation results. Simulations are performed with a surrogate model, assuming periodic unit cells and a constant wall thickness over the array. The mechanical material parameters of the base material TPU were obtained in uniaxial tensile tests.

At first, a uniform single layer, made from a unit cell array with five cells in width and ten cells in length, is simulated (Figure 4a,c). Section 5 and the Supporting Information describe the detailed parameters of the geometries, the test conditions, and bonding tests between the layers. The simulation predicts an auxetic deformation (in the z -direction) with a small warping in-plane and a curving out-of-plane in the y -direction (Figure 4c). For the experimental validation of the simulation, a uniform single layer was manufactured with a thermoforming process and tested in a tensile test (Figure 4b). The image series shows the expected auxetic behavior (z -direction). The last image of the series shows the curving out-of-plane with simultaneous warping in-plane of the uniform part-unit cell array (occurring reflections in the two rightmost pictures in Figure 4b). In a second step, multilayer samples, made from uniform unit cell arrays, were investigated. The image series (Figure 4e) of a 40-layered uniform unit cell array shows the auxetic behavior during tensile testing. Video S1, Supporting Information, shows the experimental implementation of the 40-layered uniform unit cell array. The experiment furthermore shows the absence of warping and curving, as the interaction between the joined layers prohibits out-of-plane deformations. The simulation results (Figure 4c,f) show that with elongation, the samples shrink in thickness

(y -direction) close to the edge. A comparison of the simulation in the z -direction between the single and multilayer sample shows a reduction in the displacement values. The displacement of the stacked structure (Figure 4d) is inhibited by the stretching of the flatter structure and is consequently lower than the displacement of the higher structure (Figure 4a).

The maximum visible transversal strain in the middle of the samples was measured by optical methods and compared to analytical values based on Equation (1) as well as simulation results (Figure 5). The transversal strain referring to the analytical model

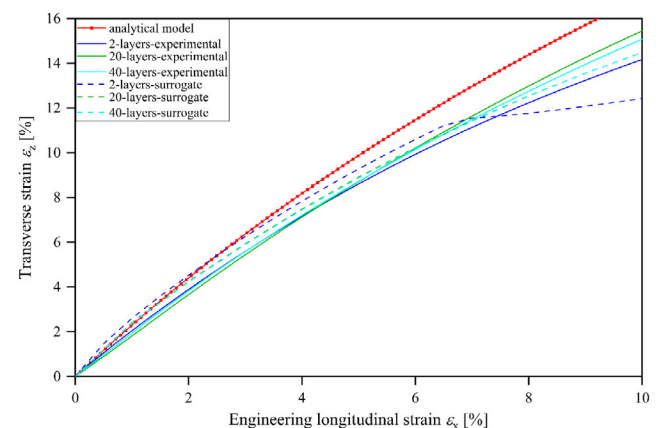


Figure 5. Transverse strain over engineering longitudinal strain of differently stacked layers experimental measurements compared to the analytical model and the simulation with a surrogate model.

is an upper boundary as it assumes an infinitely large sample with rigid parallelograms that only unfold and do not distort.

The analytical solution, experimental measurements, and simulation results agree well for small deformations, as edge effects, sample geometry, and clamping have little effect. For larger deformations, the measurement and simulation naturally show a smaller strain in the z -direction, as clamping hinders the lateral deformation, and the stress state at the edges impacts deformation compared to an infinitely large sample.

The engineering longitudinal strain refers to the complete sample length, while the local strain was not analyzed. For engineering longitudinal strains higher than 4.3%, the transversal strain of the two layers is lower than the transversal strain of the 20 and 40 stacked layers. For stacks with more than two layers, the out-of-plane warping is hampered by the chosen sample geometry. The joined layers increase the bending stiffness and therefore prevent out-of-plane deformation in the transversal direction. The simulated transversal strain for a two-layer sample shows a kink at an engineering longitudinal strain of 6% and describes the simultaneous warping effect. In the simulation, this effect occurs abruptly, as

expected for buckling in the transversal direction and idealized behavior. However, in experiments, the transition is not as abrupt which is probably related to the rather large thermoformed structures relative to the sample size. In experiments, the transition starts at lower engineering longitudinal strains. Here, the clamping of the two layers prevents an optimal deformation in the clamping area. Nevertheless, the surrogated model shows good agreement with the experimental values for strains up to 6%.

To enable more complex shape morphing for realistic applications, multilayer samples where the unit cell geometry changes within are investigated. In the first example of a nonuniform part-unit cell array the offset V is varied over the x -coordinate as described in Figure 1d. The offsets of the part-unit cells are meant to create a shape morphing from a straight to a bulged structure based on locally different auxetic behavior. The nonuniform unit cell arrays are also investigated under tension in the x -direction with optical evaluation and compared to simulation results.

The nonuniform unit cell array in Figure 6a shows the potential of the structure for shape morphing by a higher

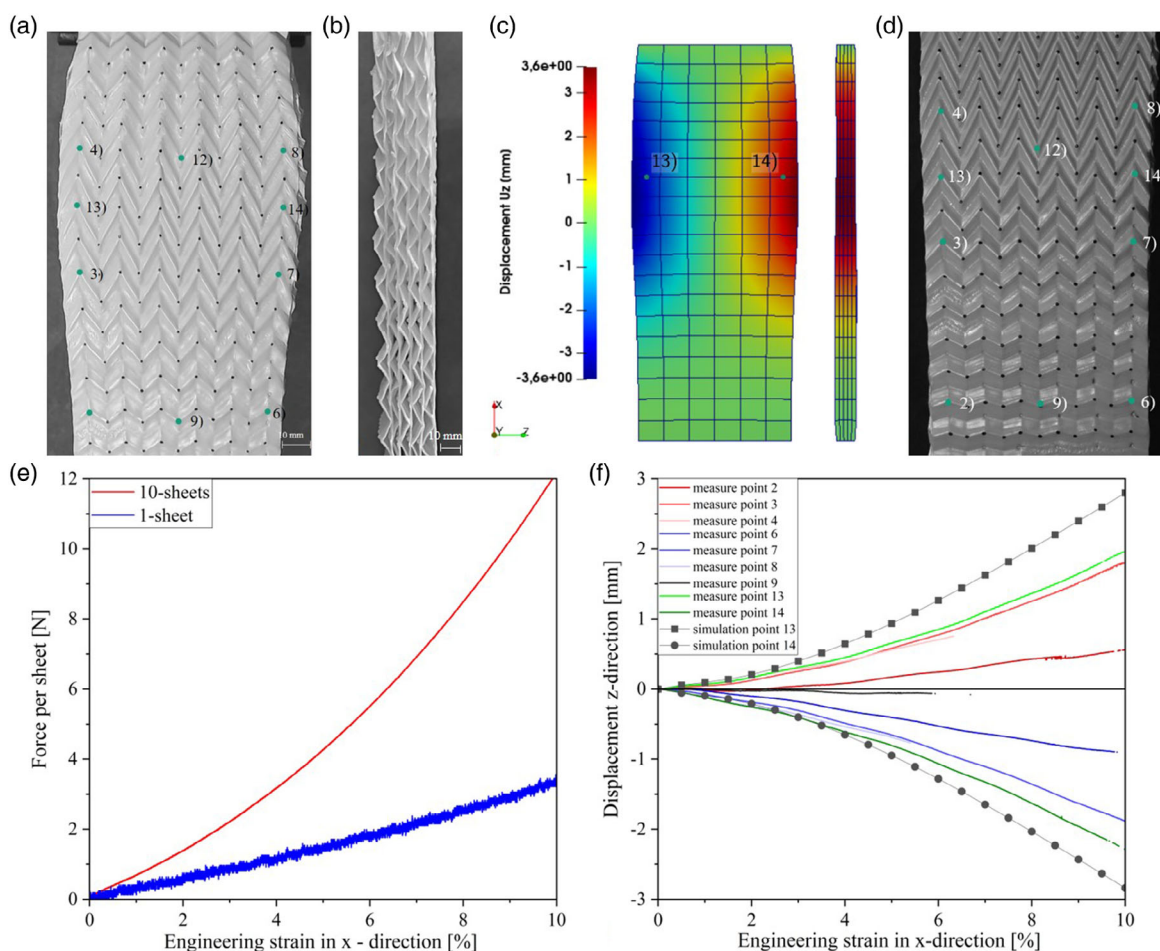


Figure 6. Results of the tensile test of the nonuniform unit cell array with ten layers, a) top and b) side view of the nonuniform unit cell array at 20% engineering strain, c) deformed model and displacement field in the z -direction (u_z) at 10% engineering strain, d) deformation of the nonuniform unit cell array at an engineering strain of 10%, e) force per layer for a nonuniform part-unit cell array and the nonuniform unit cell array and f) comparison of displacement in the z -direction at selected markers (see (b)) from the measurements by optical evaluation and the simulation using a surrogate model.

displacement. Compared to the initial width of the structure, the used design parameters generate a structure widening of 20% at the widest point. Figure 6b shows the side view of the structure at an engineering strain of 20%. The structure exhibits a complete stretching of the lower layer, which means that the auxetic deformation in these areas is decreased due to increased stiffness of these cells. After the complete stretching of the lower uniform part-unit cell array, the subsequent guarantee of the auxetic behavior of the higher uniform part-unit cell array is only possible because the TPU material can deform with it. If very stiff materials were used instead a locking of the unit cells due to their incompatibility (geometric frustration), would lead to material failure. Figure 6e shows the force per layer over the engineering strain of a high nonuniform part-unit cell array and a ten-layer nonuniform unit cell structure where the force has been divided by the number of layers. The curve of the ten-layer uniform unit cell structure shows a higher increase of the force per layer than the uniform part-unit cell layer which results may be from the suppressed out-of-plane deformation. The comparison between the simulation and the experiments was carried out up to a strain of 10%, since a sufficiently good optical evaluation was practicable up to this point. Figure 6c,d show the simulated displacements in the transversal z -direction and the experimental evaluation at a strain of 10%. Additionally, Figure 6d describes the measure points for the optical evaluation. The displacements in the z -direction were obtained by optical evaluation at different measurement points versus the engineering strain in the x -direction (Figure 6f). Points nine and twelve lie inside the neutral axis and have almost no displacement in the z -direction. The deviation from zero can be explained by an inaccuracy in the clamping of the sample. In contrast to measurement point nine, the auxetic behavior of the measurement points two and six is increased because they lie outside of the neutral axis. The highest values are measured at points thirteen and fourteen. The measurement points three and seven show that their curves are almost identical to points four and eight because they have an approximately equal distance from the points of largest displacement. In the diagram, the displacements in the z -direction obtained from the simulation agree well up to an engineering strain of 4%. Afterward, the deviations are most likely related

to the homogenization assumption of undistorted cells such that frustration of cells does not take place in the simulation, in contrast to the measurement.

By using a nonuniform distribution of design parameters, morphing toward a shape similar to a beer glass is established. The next step is to find a distribution of design parameters according to an a priori-defined target shape, which is achieved by an optimization of the structure. This approach is characteristic of an inverse design process.

3.3. Design Optimization for Defined Shape Morphing

The offset of the nonuniform unit cell structures from Section 3.2 changes only along the x -axis, which results in a symmetric deformation and is therefore insufficient for a complex target deformation. To create such a desired complex target deformation, the unit cell design parameters in the array must change continuously in both directions in the plane. To demonstrate the optimization of such a deformation, the solution of the example from Figure 7 is shown.

We restrict ourselves to a part-unit cell shown in Figure 1a with a varying design parameter V . The plane has 432 unit cells such that we have 432 design parameters to optimize. The dimensions of the array are

$$N_x \times N_y \times N_z = 36 \times 1 \times 12 \quad (3)$$

$$L_x \times L_y \times L_z = 360 \text{ mm} \times 5 \text{ mm} \times 169.68 \text{ mm} \quad (4)$$

where N_i and L_i are the number of cells and the length in the respective direction. The height L_y is equivalent to the height h of the single layer (see Figure 1a). We refer to the boundaries of the array by

$$X1: X = 0, \quad X2: X = L_x, \quad Z1: Z = 0, \quad Z2: Z = L_z \quad (5)$$

The boundary conditions are those of a strain-controlled tensile test with clamped boundaries on $X1$ and $X2$ and a displacement on $X2$

$$u_x(X1) = u_y(X1) = u_z(X1) = 0 \quad (6)$$

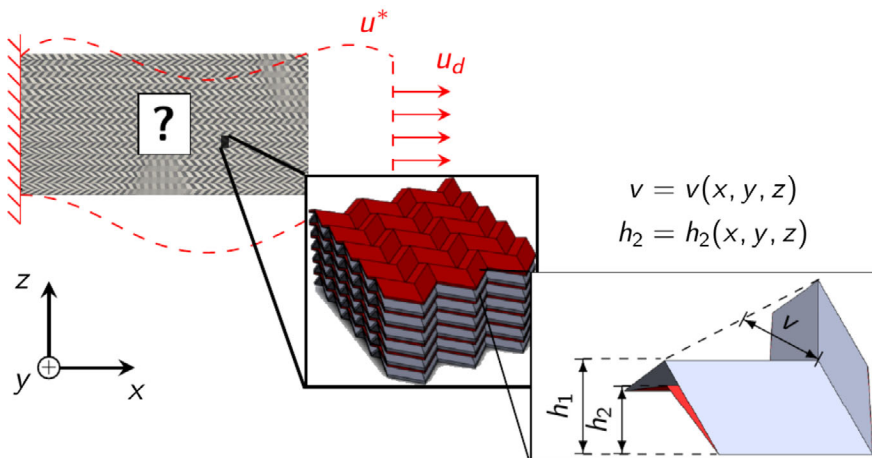


Figure 7. Multiscale optimization problem: Array of unit cells parametrized with V and h_2 and a target shape u^* .

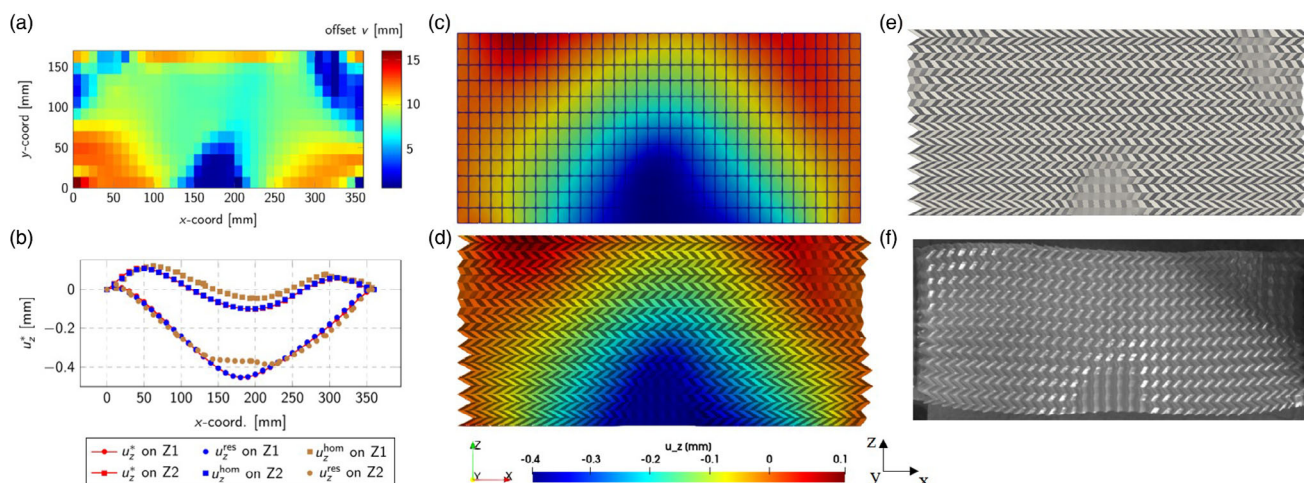


Figure 8. Results of the design optimization. a) optimal distribution of the design parameter V , b) comparison of the target function and displacements in the z -direction with the surrogate model (hom) and a resolved model (res) at 10% engineering strain, c) comparison of displacements u_z in the reduced model, d) the resolved model, e) resolved geometry, and f) the experimental sample at 10% engineering strain.

$$u_x(X2) = 1 \text{ mm} \quad (7)$$

$$u_y(X2) = u_z(X2) = 0 \quad (8)$$

The target function is the external shape shown in Figure 7 imposed by a target displacement

$$u_z(Z1, x) = f_1(X) \quad (9)$$

$$u_z(Z2, X) = f_2(X) \quad (10)$$

on the unconstrained boundaries $Z1$ and $Z2$. An extension to 3D and an optimization with different parameters V and h_2 is straightforward. For this application, however, only the parameter V is of interest as it influences the transverse deformation in the z -direction.

The geometry is discretized with hexahedral elements using one finite element per unit cell. The material behavior is represented by the surrogate model as described above. As FE-solver CalculiX is used. The optimization solver is implemented in the Julia language. The optimization converges after ≈ 20 iterations, which means that the BVP is solved 40 times during the optimization. This is done efficiently by using the reduced model. In this case, the solution of the BVP takes about 7 s on a single core with 1.80 GHz. The results of the optimization are summarized in Figure 8.

The optimal design is shown in Figure 8a as a distribution of the design parameter $V(x,z)$. It is the basis for the reconstructed geometry shown in Figure 8e. It is used as a template for the production of molds for the thermoforming process. In Figure 8b, a comparison between the target function and the displacements on the boundaries $Z1/Z2$ of the reduced model and a fully FE-model are shown. For the resolved simulation, the reconstructed geometry is discretized with approx. 2×10^5 linear shell elements and the agreement of the target function and the reduced model are very good. The difference to the resolved model is larger and mainly caused due to the violation

of periodicity. This is the case on the boundary of the macroscopic geometry and in the presence of nonuniform parameter distributions. The difference between the reduced and the resolved model is, therefore, going to vanish for increasing array sizes and smoother parameter distributions. Nevertheless, the overall distribution of u_z of the reduced and the resolved model in Figure 8c,d are very good. Figure 8f shows a first sample of the sample produced by deep-drawing during a tensile test and in a first approximation, the sample shows the desired shape change, equal to Video S2, Supporting Information. The resolved model is optimized for low deformations and a linear behavior. Because of the different offsets V , stiffness and transverse elongation of the structure varies locally, so the power distribution is not homogenous anymore. To achieve a good agreement, it is necessary for further investigations to optimize the resolved model for high deformation and for target deformation at a certain strain.

4. Conclusions

One path sketched out in this work is to integrate system functionality (here: programming shape morphing) into a single and easily-to-recycle material as well as establish a process enabling to produce m^3 in a role-to-role and layer-by-layer process. While the layer-based approach certainly carries some limitations on the unit cell designs this limitation can be overcome by further structuring the layers by stamping or more complex forming approaches.

We showed a fabrication process that can handle the complex requirements of Programmable Materials, such as highly elastic base materials, complex unit cells geometries used for logical operations and locally changing parameters. While PU-based foils offer a very simple forming process and allow for long lifetimes under large deformations in service, other polymers could be used as base materials. Since the functionalization is based on the metamaterial structure, bio-based or biodegradable polymers

can be used to further improve the environmental footprint of this concept. Furthermore, smart/functional materials can be used to implement further triggers or actuation. For example, polyurethane can be trained to show 2-way shape memory behavior, and therefore such structures could be actuated solely by a change of temperature.

In general, this study shows that the development of programmable materials with a designed behavior based on an algorithm requires a tight interaction between optimization algorithms and deep knowledge concerning manufacturing limitations. The calculation of suitable design and process parameters requires the solution of a complex multiscale optimization problem. Here, especially unstable states and the associated structural changes distributed along the material's volume require further research. Furthermore, the design space opened up in this study needs to be explored by implementing new mechanisms, reaching out to the limits in the processing parameters and functional integration, and using different materials and their combination. Since the design space is rather large, the efforts can be focused on aiming for specific functionalities (e.g., shape morphing or adaptive stiffness) and possible applications (e.g., personal safety equipment or medical devices for orthopedics).

5. Experimental Section

Simulation and Modeling Parameters: For the FEM simulations, Calculix 2.16 was used. For the modeling, a Mooney–Rivlin model with the parameters $C10 = 0$ MPa, $C01 = 6.29$ MPa, $D10^{-3} = 1$ /MPa, shell thickness = 0.4 mm was used. The material parameter identification was done in a uniaxial tension test with a constant strain rate of $5\% \text{ min}^{-1}$. The structure was modeled with linear shell elements. For the unit cell arrays, the nodes of the different layers were merged to connect them.

Optimization of Design Parameter Distribution: To obtain a manufacturable shape morphing behavior and the resulting target shape shown in Figure 7, an optimal design of the material's inner structure was found. The material's volume was subdivided into an array of individually parameterized unit cells. The goal was to find a distribution of the geometry parameters $V(x,y,z)$ and $h_2(x,y,z)$. This resulted in a complex multiscale optimization problem, equal to Figure 7. It was solved by using a surrogate-based optimization approach, as described in Lichti et al.^[20]

To find a desired shape u^* under given boundary conditions u_d , a distribution of design parameters was found. The design parameters were the geometry parameters V and h_2 in each cell and the target function is the difference between the current state and the desired state u^* . As constraint condition, the mechanical equilibrium with the given boundary conditions was fulfilled. Consequently, the evaluation of a target function involved the solution of the boundary value problem (BVP). For the solution to this optimization problem, two main challenges were tackled. First, a solution of the fully resolved geometry was computationally very expensive and not reasonable. Second, for large numbers of design variables computing the derivative with reference to the design variables was very expensive.

Therefore, an adjoint optimization approach as described by Freil^[30] was used. This facilitated computation of the gradient with reference to design variables and allowed the use of an iterative gradient descent method. The adjoint approach required the solution of a base BVP (see Figure 7 and an adjoint BVP of equal size in every iteration).

For an efficient solution of the mechanical BVP, a model reduction is performed. Instead of solving the fully resolved geometry in every optimization iteration, every unit cell is discretized by a single element with the same macroscopic behavior as the unit cell. The macroscopic behavior of the cell depends on the macroscopic loading and the design parameters as shown in Figure 2. To describe this generally nonlinear

behavior, a database for the macroscopic mechanical behavior is precomputed. Therefore, homogenized stresses of a unit cell are computed for a high-dimensional grid of data points similar to.^[19] However, the data points are not only sampled in the strain space but also the design space. Therefore, a database

$$\widehat{S}(V, h_2, \widehat{C}) = D(V, h_2, \widehat{C}) \quad (11)$$

mapping the macroscopic strain \widehat{C} and the design parameters V and h_2 to homogenized stresses \widehat{S} is obtained. In (3) S and C are the second Piola–Kirchhoff stress tensor and the right Cauchy–Green strain tensor. Intermediate states are obtained by interpolating between data points. The derivatives with respect to the strain and the design parameters are obtained by calculating the derivative of the interpolation function. For a more detailed description of the applied surrogate model, see.^[19] The precomputation of the database is computationally expensive; however, all data points are independent so that the computations can be done in parallel on a compute cluster. Based on this database, a surrogate-based optimization can be conducted resulting in an array of unit cells with a non-uniform distribution of design parameters.

Fabrication of the Samples and Experimental Methods: Thermoforming Process: A thermoplastic polyurethane film (Platilon U 2102 A) with a thickness of 500 μm from the company Covestro was used as material for the thermoforming process. In preparation for the production, the film was cut into layers (350 \times 250 mm) and clamped in the clamping frame of the thermoforming machine. The deep-drawing of the layers was performed on a thermoforming machine ILLIG KFG 37a with processing parameters $T_H = 380^\circ\text{C}$ and heat time $t = 60$ s. After the deep-drawing process, the foils had a mean thickness of ≈ 400 μm .

Fabrication of the Samples and Experimental Methods: Tensile Test: For the characterization of the uniform part-unit cell array and uniform unit cell arrays, tensile tests on a Zwick Roell with a 2 kN load cell and a testing speed of 5.61 mm s^{-1} . Between the different layers, 8 mm thick steel plates were used as spacers for the height differences between the layer. The positioning of the plates was ensured with a positioning screw. The plates and the screw prevent the structures from slipping out of the clamping blocks. For the investigation of the nonuniform part-unit cell array, the structure was extended 30 mm in length, with a test speed of 5 mm min^{-1} , and a 5 kN load cell was used. The measurements were made on an Hegewald and Peschke Inspekt table blue tensile testing machine.

Fabrication of the Samples and Experimental Methods: Optical Evaluation: The strain monitoring for the optical evaluation of the uniform part-unit cell array and uniform unit cell arrays was done by a GOM - Aramis 4M Adjustable system, a commercial 3D-DIC (digital image correlation) system, to detect the strain at any point of the specimen. For this purpose, measurement markers were placed on the surface of each specimen. Analysis lines were placed between the points to measure transverse and longitudinal elongation. Before starting the tensile test, a reference measurement was performed with a preload force of 2 N. The force signal was fed directly into the GOM system to record the force–displacement data without a delay between load and recording.

For the optical evaluation of the non-uniform unit cell array, the structure must be prepared differently because of the different local deformations. The samples are sprayed with a white varnish and a dot grid is applied to provide high contrast on the sample. In contrast to the uniform unit cell array, the nonuniform unit cell array was evaluated with a series of images and the free software of GOM correlate. For this, it was necessary to take ten pictures per second of the movement to guarantee a high mesh resolution for the optical evaluation.

Supporting Information

Supporting Information is available from the Wiley Online Library or from the author.

Acknowledgements

This work was made possible and supported by the Fraunhofer Cluster of Excellence Programmable Materials (CPM). Further thanks go to Dr. Alexander Leichner for the program for the optimization solution, which was also developed within the framework of the CPM. C. Eberl acknowledges funding by the Deutsche Forschungsgemeinschaft (DFG, German Research Foundation) under Germany's Excellence Strategy – EXC-2193/1 – 390951807.

Open Access funding enabled and organized by Projekt DEAL.

Conflict of Interest

The authors declare no conflict of interest.

Data Availability Statement

The data that support the findings of this study are available in the supplementary material of this article.

Keywords

design parameters, fabrication concept, metamaterial optimization, Miura-ori, programmable materials, shape morphing

Received: March 16, 2022

Revised: June 13, 2022

Published online:

-
- [1] S. Walker, N. Coleman, P. Hodgson, N. Collins, L. Brimacombe, *Sustainability* **2018**, *10*, 666.
- [2] L. Weisheit, F. Wenz, T. Lichti, M. Eckert, S. Baumann, C. Hübner, C. Eberl, H. Andrä, *ZWF* **2020**, *115*, 470.
- [3] O. Speck, T. Speck, *Biomimetics* **2019**, *4*, 26.
- [4] F. Wenz, I. Schmidt, A. Leichner, T. Lichti, S. Baumann, H. Andrae, C. Eberl, *Adv. Mater.* **2021**, 2008617.
- [5] M. F. Berwind, A. Kamas, C. Eberl, *Adv. Eng. Mater.* **2018**, *20*, 1800771.
- [6] C. A. Aubin, B. Gorissen, E. Milana, P. R. Buskohl, N. Lazarus, G. A. Slipper, C. Keplinger, J. Bongard, F. Iida, J. A. Lewis, R. F. Shepherd, *Nature* **2022**, *602*, 393.
- [7] P. Jiao, A. H. Alavi, *Int. Mater. Rev.* **2021**, *66*, 365.
- [8] S. C. L. Fischer, L. Hillen, C. Eberl, *Mater.* **2020**, *13*, 3605.
- [9] M. J. Mirzaali, S. Janbaz, M. Strano, L. Vergani, A. A. Zadpoor, *Sci. Rep.* **2018**, *8*, 965.
- [10] Y. Han, W. Lu, *Mater. Des.* **2018**, *141*, 384.
- [11] P. Fratzl, K. Jacobs, M. Moller, T. Scheibel, K. Sternberg, *Materialforschung: Impulsgeber Natur—Innovationspotenzial biologisch inspirierter Materialien und Werkstoffe* (acatech DISKUSSION), utzverlag, München **2019**.
- [12] K. Luan, A. West, E. DenHartog, M. McCord, *Textile Res. J.* **2020**, *90*, 617.
- [13] L. Xu, T. C. Shyu, N. A. Kotov, *ACS Nano* **2017**, *11*, 7587.
- [14] H. Fang, S. Li, H. Ji, K. W. Wang, *Phys. Rev. E* **2017**, *95*, 52211.
- [15] A. L. Wickeler, H. E. Naguib, *Mater. Des.* **2020**, *186*, 108242.
- [16] M. Schenk, S. D. Guest, *Proc. Natl. Acad. Sci. USA* **2013**, *110*, 3276.
- [17] F. Feyel, *Comput. Meth. Appl. Mech. Eng.* **2003**, *192*, 3233.
- [18] J. Köbler, M. Schneider, F. Ospald, H. Andrä, R. Müller, *Comput. Mech.* **2018**, *61*, 729.
- [19] J. Yvonnet, E. Monteiro, Q.-C. He, *Int. J. Mult. Comp. Eng.* **2013**, *11*, 201.
- [20] T. Lichti, A. Leichner, H. Andrä, R. Müller, F. Wenz, C. Eberl, A. Schwarz, C. Hübner, *Int. J. Solids Struct.* **2022**, 111769.
- [21] Z. Lin, L. S. Novelino, H. Wei, N. A. Alderete, G. H. Paulino, H. D. Espinosa, S. Krishnaswamy, *Small* **2020**, *16*, 2002229.
- [22] Y. Hou, Y. Wang, M. Yu, Z. Wang, H. Yu, *Adv. Mater. Technol.* **2020**, *5*, 2000249.
- [23] S. Liu, G. Lu, Y. Chen, Y. W. Leong, *Int. J. Mech. Sci.* **2015**, *99*, 130.
- [24] M. Schenk, S. D. Guest, G. J. McShane, *Int. J. Solids Struct.* **2014**, *51*, 4196.
- [25] J. Ma, J. Song, Y. Chen, *Int. J. Mech. Sci.* **2018**, *136*, 134.
- [26] S. Sengupta, S. Li, *J. Intell. Mater. Syst. Struct.* **2018**, *29*, 2933.
- [27] M. Khorram Niaki, F. Nonino, G. Palombi, S. A. Torabi, *JMTM* **2019**, *30*, 353.
- [28] T. Pereira, J. V. Kennedy, J. Potgieter, *Proc. Manufact.* **2019**, *30*, 11.
- [29] J. U. Surjadi, L. Gao, H. Du, X. Li, X. Xiong, N. X. Fang, Y. Lu, *Adv. Eng. Mater.* **2019**, *21*, 1800864.
- [30] S. Frei, H. Andrä, R. Pinnau, O. Tse, *Comput. Optim. Appl.* **2015**, *62*, 111.